1-1-1997

Preferential Bonding Orientations of Ferrocene on Surfaces

C. Waldfried

D. Welipitiya

C. W. Hutchings

H. S. V. de Silva

Gordon A. Gallup
University of Nebraska - Lincoln, ggallup1@unl.edu

See next page for additional authors

Preferential Bonding Orientations of Ferrocene on Surfaces

C. Waldfried, D. Welipitiya, C. W. Hutchings, H. S. V. de Silva, G. A. Gallup, and P. A. Dowben*

Department of Physics and Astronomy and Center for Materials Research and Analysis, University of Nebraska−Lincoln, Lincoln, Nebraska 68588-0111

W. W. Pai, Jiandi Zhang, and J. F. Wendelken

Solid State Division, Oak Ridge National Laboratory, Oak Ridge, Tennessee 37831-6030

N. M. Boag

Department of Chemistry, Salford University, Salford, M5 4WT England

Received: July 30, 1997[⊗]

We have measured the molecular orientation and bonding of adsorbed ferrocene on Ag(100) and Cu(100) using angle-resolved photoemission spectroscopy (ARPES). The results for molecular adsorption on Ag(100) are complemented by high-resolution electron energy loss spectroscopy (HREELS) measurments and ab initio calculations for the ferrocene vibrational modes. The measurements indicate that ferrocene adsorbs on Ag(100) with the molecular axis perpendicular to the surface. In contrast, as indicated using ARPES and scanning tunneling microscopy, ferrocene adsorbed on the Cu(100) surface is oriented with the molecular axis *parallel* with the surface. Model calculations allow us to assign all of the observed vibrational modes for the weakly bound molecular ferrocene on Ag(100)−both dipole and impact scattering modes have been observed.

Introduction

Metallocenes, including ferrocene (schematically shown in Figure 1), are central to inorganic organometallic chemistry and are important catalysts.[1] Metallocenes have also been recently used as metallization sources,[2−4] but as yet only a few studies with a focus on the surface chemistry of metallocenes exist.[5−7] Ferrocene, $Fe(C_5H_5)_2$, has been demonstrated to adsorb molecularly on Ag(100) at low temperatures[5,6] as a weakly bound molecular adsorbate.[5]

As noted in recent reviews,[8,9] electron spectroscopies in conjunction with dipole selection rules and symmetry arguments may be used to study the preferential bonding orientation of large molecular adsorbates on surfaces. The use of symmetry and selection rules in determining molecular orientation originally focused on small, diatomic molecules such as CO, N_2, and NO on metal and semiconductor surfaces. The use of angle-resolved photoemission (ARPES) has been extended to determine the preferential surface bonding orientation of large organics,[8−10] main group cluster molecules[8,11] and organometallics.[8,9,12]

Although ARPES is a powerful tool for studying molecular adsorbates, it has several limitations. The application of symmetry and selection rules to photoemission may not always uniquely define the adsorption site. Furthermore, photoemission tends to be insensitive to dehydrogenation in large molecules. Thus, high-resolution electron energy loss spectroscopy (HREELS) is an excellent complementary spectroscopy. There is also the complication that the adsorbed ferrocene species could adopt either one of the two possible local symmetry configurations: D_{5d} or D_{5h} (as shown in Figure 1). Of course, interaction with the substrate will lead to a reduction in the absolute point group symmetry.

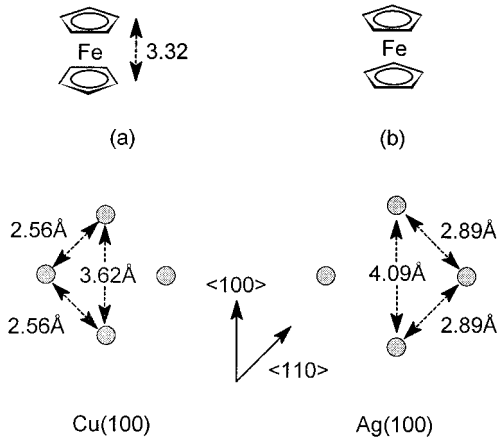

Figure 1. The two configurations of ferrocene: (a) staggered configuration of D_{5d} symmetry and (b) eclipsed configuration of D_{5h} symmetry. The schematic of the surface lattice of both Cu(100) and Ag(100) is also shown.

Experimental Section

The angle-resolved photoemission spectra (ARPES) were acquired at the Synchrotron Radiation Center in Stoughton, WI. The light was dispersed using the 6 m toroidal grating monochromator (TGM), and several photon energies were used. The ultrahigh-vacuum chamber was equipped with an angle-resolved hemispherical electron energy analyzer which has an acceptance angle of ±1°, as described elsewhere.[13] The combined energy resolution of the analyzer and the light source was approximately 150 meV or less. The light polarization dependence of the photoemission spectra was studied at two light incidence angles: 70° off-normal (p-polarized light) and 40° off-normal ((s + p)-polarized light). While considerable numbers of spectra were taken at various emission angles, all the photoemission spectra shown in this paper were acquired

* Address all correspondence to this author.
[⊗] Abstract published in *Advance ACS Abstracts,* September 15, 1997.

S1089-5647(97)02496-6 CCC: $14.00

with the photoelectrons collected normal to the surface. The base pressure of the system was maintained at 1×10^{-10} Torr. The Ag(100) and Cu(100) single crystals were mounted on a cryostat in the analysis chamber with the capability of liquid nitrogen cooling and resistive heating. The temperature was monitored with a K-type (chromel−alumel) thermocouple, and both substrates could be cooled to 150 K. The substrates were cleaned by repeated Ar^+ ion sputtering and annealing as noted elsewhere.[5] Ferrocene was sublimed from the solid and admitted into the chamber through a standard leak valve.

The high-resolution electron energy loss (HREELS) spectra were taken in a separate UHV (HREELS) chamber with a base pressure of 8×10^{-11} Torr and an LK-2000 angle-resolved electron energy loss spectrometer. An electron beam with an energy of 1.85 eV was incident at an angle of 60° off the surface normal throughout this work. Spectra were obtained in both specular and off-specular ($\Delta\theta = 9°$) directions following a ferrocene exposure of 2 langmuirs (1langmuir $= 1 \times 10^{-6}$ Torr s) on Ag(100) at 110 K.

The scanning tunneling microscope low-temperature (STM) images of ferrocene on Cu(100) were collected using an Omicron STM system in a third UHV system. Submonolayer coverages of ferrocene on Cu(100) were adsorbed at room temperature following a ferrocene exposure of 10^3 langmuirs. Images were acquired using a sample bias of $V_{bias} = +2$ V with a tunneling current of $I_t = 0.5$ nA in the traditional current mode.

Theory

Theoretical calculations were performed to model the ferrocene vibrational modes using the Gaussian-92 ab initio package.[14] Calculations were undertaken with the standard STO-3G minimal basis set and the extended 3-21G basis set. The initial geometry of ferrocene was determined by assigning the molecule to the D_{5d} symmetry point group and standard bond lengths. Optimization of this geometry at the self-consistent-field (SCF)[15] level using the STO-3G basis set resulted in convergence. The SCF-STO-3G optimized geometry was further refined at the SCF-3-21G level and produced a stable minimum retaining the D_{5d} symmetry. The solutions of the improved force field calculations provide the vibrational frequencies of ferrocene summarized in Table 1. This level of calculation was repeated for deuterated ferrocene (ferrocene-d_{10}), which is also shown in Table 1. Throughout this article point group representation elements of vibrational modes are denoted by upper case letters and for molecular orbitals by lower case letters.

Ag(100). The orientation of ferrocene adsorbed on Ag(100) at 150 K as a function of exposure was studied with ARPES (Figures 2 and 3). Panel a shows spectra measured with p-polarized light, and panel b shows spectra acquired with (s + p)-polarized light. The angle-resolved photoemission spectra, in general, resemble those of the angle-integrated studies reported earlier.[5,6] These angle-resolved photoemission spectra binding energies are referenced to the Ag(100) Fermi energy, and because of greater resolution and angular resolution, the binding energies differ slightly from previous work[4,5] (Table 2).

Upon adsorption of ferrocene, suppression of the Ag 4d bands and growth of photoemission features at approximately 4.1, 5.4, 7.0 , 8.9, 10.9, 13.4, and 17.0 eV is observed (Figures 2 and 3) as summarized in Table 2. There exists a strong similarity between the gas-phase photoemission spectra of ferrocene and condensed ferrocene,[5] although the molecule to substrate and intermolecular interactions have been observed to shift, split, or broaden the observed energies of the molecular orbitals. On the basis of theoretical calculations of the ground-state molecular orbitals of ferrocene[16−22] as well as gas-phase photoemission and ionization potential studies,[23−27] we can assign the adsorbed ferrocene-induced photoemission features to the molecular orbitals of ferrocene (Table 2, Figures 2 and 3). The features at 5.4 and 4.1 eV arise from the ferrocene $8a_{1g}$ and $4e_{2g}$

TABLE 1: Calculated Vibrational Modes of Ferrocene and Deuterated Ferrocene Using the Extended Basis Set (3-21G) As Described in the Text

vibrational losses (meV)			
$Fe(C_5H_5)_2$	$Fe(C_5D_5)_2$	sym	vib mode
1.4	1.3	A_{1u}	ring torsion
16.1	14.9	E_{1u}	asymmetric ring tilt
30.5	28.9	A_{1g}	metal−ring stretch
40.4	36.9	E_{1g}	symmetric ring tilt
52.3	50.4	E_{1u}	$\delta(M(Cp)_2)$
53.8	52.2	A_{2u}	$\upsilon_{as}(M(Cp)_2)$
79.1	70.9	E_{2u}	π(CH)
82.1	72.4	E_{2g}	π(CH)
108.6	81.4	A_{2u}	π(CH)
111.1	82.9	A_{1g}	π(CH)
111.7	87.4	E_{1g}	π(CC)
115.8	90.4	E_{1u}	π(CH)
119.7	97.8	E_{2u}	π(CH)
119.9	101.4	E_{2g}	δ(CC)
124.1	102.6	E_{2u}	π(CC)
126.5	102.8	E_{2g}	π(CH)
136.1	105.7	E_{1g}	π(CC)
136.9	106.3	E_{1u}	π(CH)
145.5	119.9	E_{2u}	π(CC)
146.6	120.3	E_{2g}	δ(CH)
148.4	140.8	A_{2u}	δ(CH)
148.9	141.2	A_{1g}	δ(CH)
177.2	139.01	A_{2g}	ring breathing
177.3	139.05	A_{1u}	υ(CH)
182.8	175.3	E_{2u}	π(CH)
185.8	176.9	E_{2g}	δ(CH)
195.8	179.0	E_{1g}	δ(CH)
196.0	177.4	E_{1u}	π(CH)
425.4	314.5	E_{2u}	π(CH)
425.5	314.7	E_{2g}	δ(CH)
427.5	316.7	E_{1g}	π(CH)
427.6	316.8	E_{1u}	π(CH)
429.7	320.21	A_{2u}	δ(CH)
429.8	320.22	A_{1g}	δ(CH)

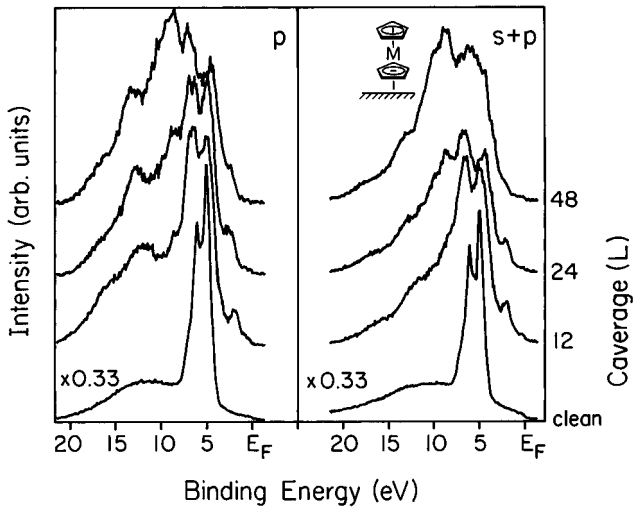

Figure 2. Coverage-dependent angle-resolved photoemission spectra of ferrocene on Ag(100) at 150 K using a 50 eV incident beam with normal emission. The spectra in panel (a) were measured using p-polarized light. The spectra in panel b were measured using (s + p)-polarized light.

TABLE 2: Molecular Orbital Binding Energies (eV) for Ferrocene[a]

molecular orbitals	theory	gas phase	Ag(100)	Cu(100)
$8a_{1g}$	7.46[16]	6.88[23]	5.4	not resolved from $4e_{2g}$
	10.1[17]	6.85[24]		
	7.9[18]	6.9[25]		
	6.45[19]	6.86[26]		
	6.7[20]	6.86[27]		
	7.6[21]			
	6.6[22]			
$4e_{2g}$	5.69[16]	7.23[23]	4.1	4.2
	8.3[17]	7.21[24]	4.6[5,6]	
	8.5[18]	7.23[25]		
	6.6[19]	7.21[27]		
	6.7[20]			
	6.7[22]			
$6e_{1u}$	8.85[16]	8.72[23]	7.0	7.1
	11.1[17]	8.72[24]	7.3[5,6]	
	9.3[18]	8.72[25]		
	8.53[19]	8.77[27]		
	8.6[20]			
	12.6[21]			
	8.6[22]			
$4e_{1g}$	8.79[16]	9.38[23]	not resolved from $6e_{1u}$	not resolved from $6e_{1u}$
	11.2[17]	9.17[24]		
	9.7[18]	9.38[25]		
	7.96[19]	9.28[27]		
	8.1[20]			
	14.58[21]			
	7.2[22]			
$6a_{2u}$	13.03[16]	12.3[23]	8.9	8.9
	15.5[17]	12.2[25]	9.3[5,6]	
	11.7[18]	12.2[27]		
$3e_{2u}$, $3e_{2g}$, $3e_{1g}$, $5e_{1u}$ and $7a_{1g}$	13.6[16]	13.0[23]	10.9	not resolved from $6a_{2u}$
	11.6[18]	13.46[23]	11.9[5,6]	
		13.6[25]		
		13.3[27]		
$5a_{2u}$, $6a_{1g}$, $2e_{2u}$, and $2e_{1g}$		16.5[23]	13.4	13.1
		16.4[25]	14.1[5,6]	
		16.6[27]		
		19.5[27]	17.0	16.3
			18[5,6]	

[a] The binding energies for theory and gas-phase experimental measurements are relative to the vacuum level. Those for the condensed phase are taken from ref 4 and referenced to the Fermi level.

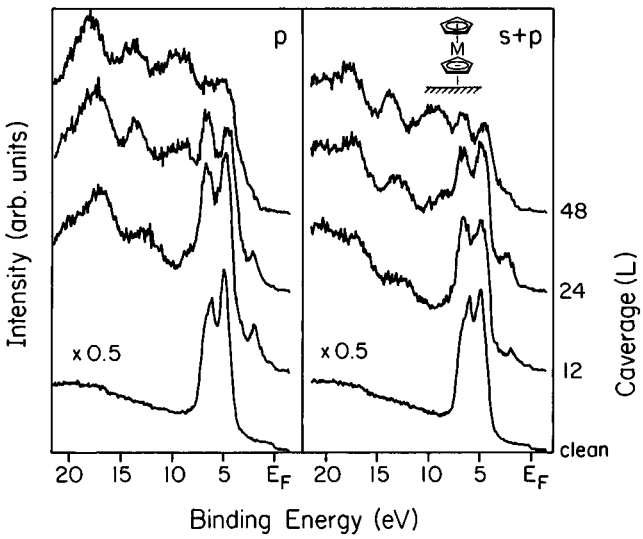

Figure 3. Coverage-dependent angle-resolved photoemission spectra of ferrocene on Ag(100) at 150 K using a 60 eV incident beam with normal emission. The spectra in panel a were measured using p-polarized light. The spectra in panel b were measured using (s + p)-polarized light.

molecular orbitals, respectively. The $6e_{1u}$ and $4e_{1g}$ molecular orbitals result in the 7.0 eV feature. The feature at 8.9 eV binding energy (the $6a_{2u}$ molecular orbital) and the prominent shoulder at 10.9 eV binding energies have contributions from a combination of molecular orbitals ($3e_{2u}$, $3e_{2g}$, $3e_{1g}$, $5e_{1u}$, and $7a_{2g}$) as is the case for the 13.4 eV feature ($5a_{2u}$, $6a_{1g}$, $2e_{2u}$, and $2e_{1g}$). The feature at 17.0 eV is primarily of carbon 2s in origin. The peak at 2.2 eV has not been uniquely identified but may result from the interfacial reaction between ferrocene and the surface (or cyclopentadienyl fragments), since it is well-resolved at low coverages.

The 5−6 eV feature is assigned to the $8a_{1g}$ molecular orbital on the basis that this feature shows the same light polarization dependence as the 17.0 eV feature. The distinct separation of the $8a_{1g}$ from the $4e_{2g}$ molecular orbital indicates that the $8a_{1g}$ is a bonding orbital and no longer the highest occupied molecular orbital.

In spectra obtained using (s + p)-polarized light (shown in Figures 2b and 3b), relative peak intensities corresponding to various molecular orbitals change significantly when compared to those using p-polarized light (Figures 2a and 3a). The peaks at 5.4, 13.4, and 17 eV decrease in intensity compared to the p-polarized spectra, while the 7, 8.9, 10.9, and 13.1 eV features remain unchanged or increased. These latter features are primarily of e_1 and e_2 symmetry, while the 5.4, 13.4, and 17.0 eV features contain substantial a_1 character. This enhancement of the fully symmetric molecular orbitals in p-polarized light is strongly indicative of a molecular orientation along the surface normal.

Figure 4 shows the HREELS spectra of ferrocene on Ag-(100) at 110 K. In the specular direction, the spectra exhibit

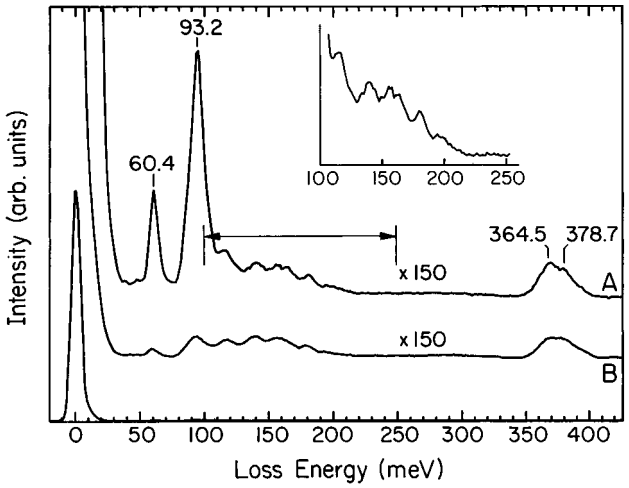

Figure 4. Electron energy loss spectra for ferrocene adsorbed on Ag(100) at 110 K. The spectra were taken following 2 langmuir exposure. Both the specular (A) and off-specular (B, $\Delta\theta = 9°$) spectra are shown with the same scale but magnified by 150 as compared to the specular elastic peak. The inset shows features in the range from 100 to 250 meV. The intensities of the two dipole-active modes ν_{as} $(M(Cp)_2)$ and π(CH), at 60.4 and 93.2 meV, respectively, are greatly suppressed in the off-specular geometry while the peaks at 364.5 and 378.7 meV are not.

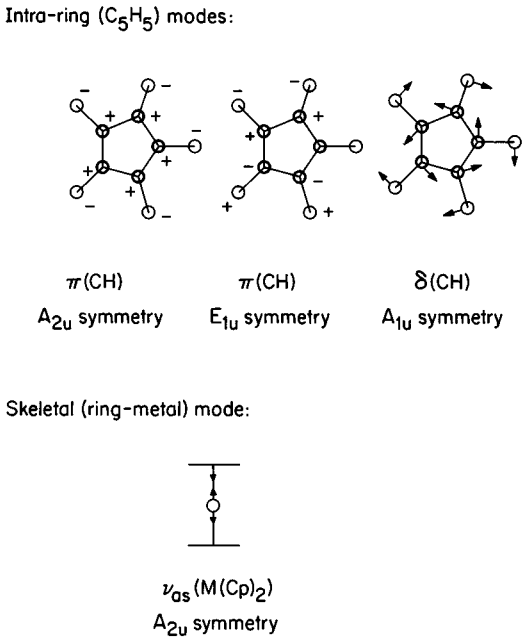

Figure 5. Normal modes of vibration for the loss peaks in the HREELS spectrum of ferrocene.

strong peaks located at 60.4, 93.2, 364.5, and 378.7 meV with a number of weaker loss features in the range 100−200 meV. The spectrum acquired in the off-specular geometry is characterized by the suppression of the 60.4 and 93.2 meV features while all the other peaks remain largely unchanged. Clearly, the 60.4 and 93.2 meV losses are strongly dipole-active modes.

We adopted the D_{5d} structure in our model calculations and for assignment of the vibrational losses. The intra-ring (Cp) modes follow vibrations consistent with the D_{5h} symmetry group, and skeletal modes follow vibrations consistent with the D_{5d} symmetry group. The symmetry and schematic representation of the important vibrational modes are indicated in Figure 5.

On the basis of our calculations, we assign the vibrational loss peak at 60.4 meV to the antisymmetric skeletal vibrational mode of the metal (M) atom and cyclopentadienyl rings (Cp), $\upsilon_{as}(M(Cp)_2)$, of A_{2u} symmetry. Similarly, the peak at 93.2 meV is assigned as the out-of-plane vibrational mode of the C−H bond, π(CH), which is also of A_{2u} symmetry. A weak A_{2u} symmetry dipole-active mode is observed at 364.5 meV. Both theory and experiment are in very good agreement, as seen in Table 3.

TABLE 3: Vibrational Modes of the HREEL Spectrum of Ferrocene[a]

calcd energies (meV)	sym	vib mode	obsd IR (meV)	HREELS (meV)
53.8 (31.3)	A_{2u}	$\upsilon_{as}(M(Cp)_2)$	59.3[c]	60.4[b]
			60[f]	68[g]
108.6 (117.3)	A_{2u}	π(CH)	96.1[c]	93.2[b]
			102[f]	101[g]
119.7 (114.9)	E_{2u}	π(CH)	118.2[d]	115.0[b]
136.9 (145.5)	E_{1u}	π(CH)	137.4[c]	140.0[b]
			138[f]	135[g]
148.4 (158.8)	A_{2u}	δ(CH)	155.5[e]	155.0[b]
182.8 (200.3)	E_{2u}	π(CH)	183.0[d]	180.0[b]
			176[f]	170[g]
196.0 (211.6)	E_{1u}	π(CH)	200.8[c]	195.0[b]
				205[g]
429.7 (471.0)	A_{2u}	δ(CH)	387[f]	378.7[b]
				390[g]
427.6 (468.9)	E_{1u}	π(CH)		364.5[b]
				353[g]

[a] Calculated vibrational modes of ferrocene under 3-21G (STO-3G) are listed in meV. Calculations show better agreement with the extended basis set: see text. [b] This work [c] Taken from ref 28 [d] Taken from ref 29. [e] Taken from ref 30. [f] Taken from ref 31. [g] Taken from ref 25.

Both specular and off-specular spectra (Figure 4) show weak losses in the range from 100 to 200 meV, which remain largely the same in intensity in both geometries. This suggests that these peaks correspond to impact (nondipole) scattering modes. The selection rules for HREEL spectroscopy favor E_{1u} and E_{2u} symmetries for nondipole-active modes, and we have made our assignments accordingly except for one A_{2u} dipole mode. The experimental losses are in-plane and out-of-plane bending mode vibrations of the C−H bond as seen in Table 3 and are in good agreement with theory.

Our calculated vibrational energies at 53.8, 108.6, and 196.0 meV are consistent with the vibrational loss peaks at 60.4, 93.2, and 195.0 meV, respectively. These values also agree with the IR data[28] for gaseous ferrocene at 59.3, 96.1, and 200.8 meV, respectively. For cyclopentane (C_5H_{10}) in crystal form, the IR data[29] find features at 118.2 and 183 meV. These agree with our calculated values at 119.7 and 182.8 meV and the HREELS data as indicated in Table 3. We therefore assign these losses in our HREELS data to C−H modes. Our calculations indicate that these two peaks correspond to π(CH) modes. A peak is observed at 155.5 meV in the IR data for crystalline ferrocene.[30] This agrees with the calculated value at 148.4 meV and the HREELS vibrational loss peak at 155 meV and, in principle, should be a dipole-acitve mode.

The peaks at 364.5 and 378.7 meV should correspond to a dipole-active mode and an impact scattering mode, respectively. The 364.5 meV mode is indeed enhanced in the specular geometry while the other loss feature remains largely the same in intensity in both geometries. These two modes can be assigned as a δ(CH) mode of A_{2u} symmetry and a π(CH) vibrational mode of E_{1u} symmetry. In the infrared data of ferrocene in solution,[31] an absorption at 387 meV, has been observed, while these losses have also been observed in high-resolution photoemission[25] at 353 and 390 meV respectively. We note that the calculated values and the HREELS loss

energies of these peaks are not in good agreement. It is difficult to explain the vibrational losses at 242, 278, and 316 meV observed in the gas-phase photoemission[25] as anything except as overtones: these losses have no calculated counterpart.

In addition to the vibrational modes for the HREELS peaks, we can assign other observed IR and Raman modes for ferrocene from the literature. The symmetries A_{1g}, A_{2g}, E_{1g}, and E_{2g} correspond to Raman-active modes while E_{2u} corresponds to inactive IR modes. Overall, we have been able to assign modes of A_{1g}, A_{2g}, E_{1g}, E_{2g}, and E_{2u} symmetries.

The energy range from 15 to 55 meV is dominated by skeletal (metal−ring) modes. The two asymmetric ring tilt modes at 16.1 and 52.3 meV have E_{1u} symmetry. The 16.1 meV mode agrees with solution IR data[31] for ferrocene at 21 meV, and the 52.3 meV mode agrees with IR data[28] for ruthenocene in solution. The metal−ring stretch mode at 30.5 meV is of A_{1g} symmetry and agrees with Raman data[28] for ferrocene-d_{10} in solution. The symmetric ring tilt mode at 40.4 meV is of E_{1g} symmetry and agrees with Raman data[28] for ferrocene in solution. The observed gas-phase electron energy loss at 35 meV, in high-resolution photoemission,[25] may be assigned to either A_{1g} or E_{1g} vibrational modes.

There is a ring breathing mode of totally symmetric representation, A_{2g}, at 177.2 meV. This agrees with Raman data[29] for cyclopentane in crystal form. The two out-of-plane bending modes at 111.1 and 111.7 meV, of A_{1g} and E_{1g} symmetries, also agree with Raman data[29] for cyclopentane in liquid and crystal forms, respectively. The in-plane C−H bending modes at 148.4 and 185.8 meV, of A_{2u} and E_{2g} symmetries, respectively, agree with Raman data[29] for cyclopentane in crystal form. The out-of-plane C−C bending mode at 136.1 meV agrees with Raman data[29] for cyclopentane-d_{10} in liquid form. The calculated losses at energies 146.6 and 195.8 meV are attributed to the in-plane C−H bending modes of E_{2g} symmetry which agree with solution Raman data[28] for ferrocene.

Based on our calculations, HREELS E_{1u} π(CH) losses in the vicinity of 16.1 and 115.8 meV and an E_{2u} loss at 124.1 meV as well as an E_{1u} $\delta M(Cp)_2$ mode at 52.3 meV are expected. Recent high-resolution HREELS studies of condensed ferrocene[32] have observed these additional modes at 22.6, 100, 123.8, and 46.3 meV, respectively.

The general softening of the modes with deuteration that we have calculated has been observed. In particular, the A_{2u} mode calculated for $Fe(C_5D_5)_2$ at 81.4 meV (108.6 meV for $Fe(C_5H_5)_2$) is observed at 79 meV as opposed to 102 meV for $Fe(C_5H_5)_2$ in the same solution.[31]

Cu(100). Figure 6 shows ARPES spectra for ferrocene adsorbed on Cu(100) as a function of exposure. Panel a shows spectra measured with p-polarized light, and panel b shows spectra measured with (s + p)-polarized light.

Upon adsorption of ferrocene at 150 K, there is suppression of the Cu 3d bands and an increase of photoemission features at binding energies of approximately 4.2, 7.1, 8.9, 13.1, and 16.3 eV as seen in Figure 6 and summarized in Table 2. The spectra for ferrocene on Cu(100) are qualitatively similar to those obtained on the Ag(100) surface. Again, on the basis of theoretical calculations of the ground-state molecular orbitals of ferrocene[16−22] and gas-phase photoemission and ionization potential studies,[23−27] we can assign these photoemission features of the adsorbed species (Table 2, Figure 5). The ferrocene $8a_{1g}$ and $4e_{2g}$ molecular orbitals induce the 4.2 eV feature that overlaps with the Cu 3d bands. The $6e_{1u}$ and $4e_{1g}$ molecular orbitals result in the 7.1 eV feature. The prominent feature at a binding energy of 8.7 eV binding energy (the $6a_{2u}$ molecular orbital) is no longer distinct from the combination

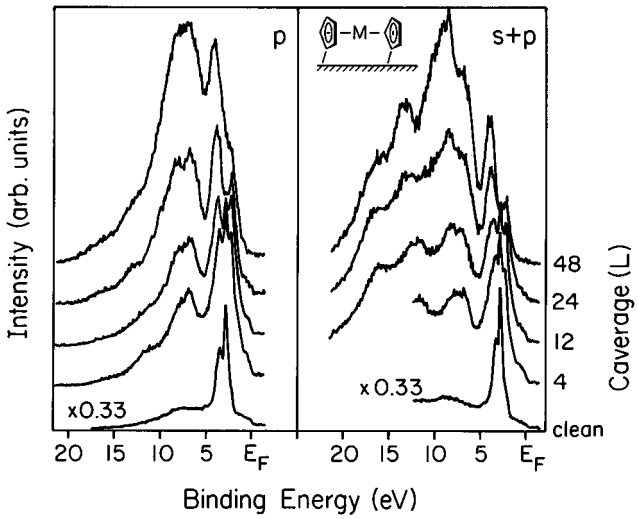

Figure 6. Coverage-dependent angle-resolved photoemission spectra of ferrocene on Cu(100) at 150 K using a 50 eV incident beam with all the photoelectrons collected along the surface normal. The spectra in panel a were measured using p-polarized light. The spectra in panel b were measured using (s + p)-polarized light.

of molecular orbitals ($3e_{2u}$, $3e_{2g}$, $3e_{1g}$, $5e_{1u}$, and $7a_{2g}$) that appear at higher binding energies. The 13.1 eV feature is also a combination of several molecular orbitals ($5a_{2u}$, $6a_{1g}$, $2e_{2u}$, and $2e_{1g}$).

For the spectra recorded with (s + p)-polarized light (Figure 6b), relative intensities of the molecular orbitals again change significantly from p-polarized light (Figure 6a), but in a slightly different manner to those of ferrocene on Ag(100). The peaks at 4.2, 8.9, 13.1, and 16.3 eV now increase (instead of decrease or remain the same) in intensity compared to the p-polarized spectra while the feature at 7.1 eV remains the same or decreases. The change in the intensity of the 8.9, 13.1, and 16.3 eV features with light polarization is opposite to the case for ferrocene on Ag(100). Since some features with substantial a_1 character increase with (s + p)-polarized light, this suggests that the molecular axis of the ferrocene is not placed perpendicular to the surface. Rather, the photoemission is consistent with a canted or "flat" molecular configuration; in other words, the ferrocene is bonded with the molecular axis tilted away from the surface normal—possibly even with the molecular axis parallel with the surface. This does not mean that there is no preferential orientation—the existence of light incident angle dependence does argue for a preferential orientation, but the specific orientation cannot be easily assigned on the basis of the angle-resolved photoemission results alone.

The scanning tunneling microscope images of ferrocene adsorbed on Cu(100) at room temperature are shown in Figure 7. The three lobes imaged in the STM are very indicative of a molecular ferrocene species oriented with the molecular axis parallel with the surface. The images indicate that the molecular axis is, in fact, along the $\langle 1\bar{1}0 \rangle$ direction. This molecular orientation is quite consistent with the angle resolved photoemission results.

No such ferrocene species could be observed on Ag(100) using scanning tunneling microscopy following large exposures of ferrocene to Ag(100) at temperatures as low as 230 K. The fact that such room-temperature adsorption is observable only for ferrocene on Cu(100) and not Ag(100) suggests that this ferrocene species is a partially dehydrogenated ferrocene. This would account for the higher effective desorption temperature than most of the molecularly adsorbed ferrocene on Cu(100) (or Ag(100) for that matter).

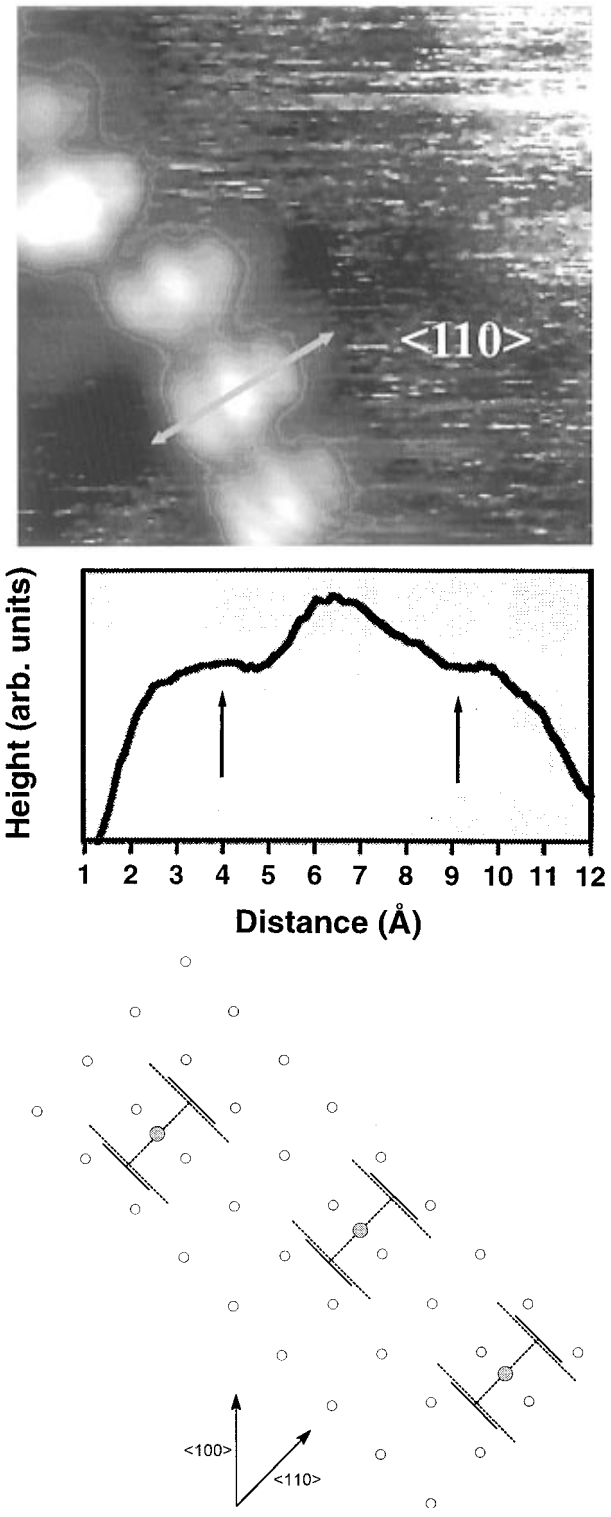

Figure 7. A constant-current STM image (4 by 4 nm) of ferrocene molecules adsorbed on Cu(100) following adsorption at room temperature. The trace through one of the adsorbed ferrocene molecules is also shown along the ⟨110⟩ direction. The relative orientation of the molecule on the Cu(100) surface is indicated schematically. (The solid line represents the 1,2-hydrogen vector, and the dotted line represents the 1,3-hydrogen vector.)

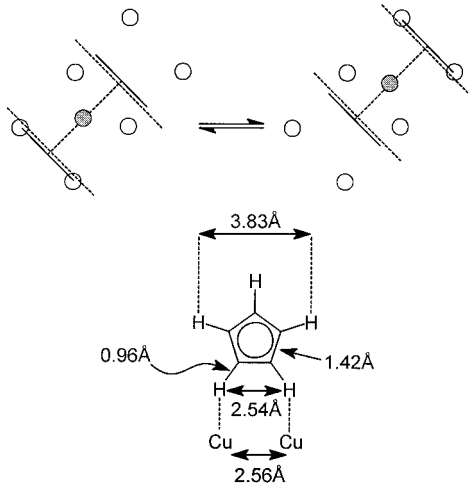

Figure 8. Schematic representation of the possible bonding configurations of ferrocene on Cu(100) consistent with the angle-resolved photoemission results following adsorption at 150 K and the STM images shown in Figure 7.

Discussion

The vibrational modes for most of the peaks in the HREEL spectra of ferrocene are reasonably modeled by our calculations based on the extended basis set (3-21G) calculations. The limited basis set (STO-3G) is less successful in modeling ferrocene. The infrared data and Raman data available in the literature support our assignments of vibrational modes of HREELS and the premise that ferrocene is a weakly bound adsorbate on Ag(100).[5] We find that adsorption of ferrocene does not result in a large perturbation of the vibrational modes. Nevertheless, the peaks found at high frequency indicate that significant improvements in the method of calculations are required. We anticipate that the use of an anharmonic force field may enhance the accuracy of the results and would allow us to better model the vibrational modes for all the peaks in the HREEL spectrum of ferrocene. Anharmonic corrections would lead to a softening of the modes, as compared to the pure harmonic potential, consistent with our data. We are currently exploring these inconsistencies through the use of ferrocene-d_{10} as a prelude to more advanced theoretical studies.

We have postulated in a previous paper[5] that molecular ferrocene is bound to Ag(100) through the plane of the cyclopentadienyl ring and resulting in a bonding orientation that places the molecular axis along the surface normal. The model calculations when compared to the HREELS data and the polarization dependence of the angle-resolved photoemission data both strongly support this contention. Bonding to the substrate occurs via a_1 orbitals as indicated by the perturbation of the $8a_{1g}$ and $6a_{1g}$ orbitals.

For Cu(100), it is very clear that a different preferential bonding orientation is adopted despite the similar chemistry of copper and silver, and we are currently undertaking experiments to elucidate these differences. We note, however, that the calculated separation between two adjacent hydrogens of an ideal cyclopentadienyl ligand (2.54 Å) is closely matched to the Cu−Cu separation of 2.56 Å compared to the corresponding Ag−Ag separation of 2.89 Å, as seen in Figure 1. A strong chelating interaction by two adjacent cyclopentadienyl hydrogens to the copper surface would therefore seem possible, as seen in Figure 8. Such an interaction would not require the molecular axis of the ferrocene to be perpendicular to the surface, in agreement with the spectroscopic results for Cu(100).

Although extraction of intermolecular distances from STM data is difficult, the observed distance between the midpoints of the external features (ca. 5.5 Å, as seen in Figure 7) is inconsistent with the separation between the cyclopentadienyl rings of ferrocene (3.32 Å), even if the molecular axis of the ferrocene was parallel to the surface. Adoption of this configuration by the ferrocene would enable the hydrogen atoms on

the unattached ring to be available for binding. However, due to the lattice separation, there are no copper atoms in an appropriate position for this to take place, as indicated by the schematic diagram in Figure 8. Nevertheless, a second energy minima is readily obtained by lengthening and ultimately cleaving the copper−hydrogen interaction of one ring by displacement of the ferrocene molecule along its axis by some 2 Å and concomitant generation of a second copper hydrogen chelating interaction through the cyclopentadienyl protons of the *second* ring. Since the energy minima are equal in energy and the barrier between them is low, the molecule will shuttle rapidly between the two paired sites, as indicated by Figure 8. Movement to adjacent paired sites is also possible; however, the barrier to this is presumably sufficiently large to permit observation of the STM images. This model provides an attractive explanation of the elongated features in the STM images of ferrocene on Cu(100) which arise from a *site-averaged environment* which increases the apparent length of the ferrocene molecule by some 2 Å.

We have been unsuccessful in obtaining STM data for ferrocene bound to Ag(100). Ferrocene is bound to the surface of Ag(100) through the π-system of the cyclopentadienyl ring with the molecular axis perpendicular to the surface. As a result, increased mobility of ferrocene over the surface of the silver when compared to the differing bonding orientation on Cu(100) is not unexpected and may be the origin of a lack of data.

It must be realized that the experiments detailed in this paper cannot detect dehydrogenation of the cyclopentadienyl ligands, and while the $8a_{1g}$ and $6a_{1g}$ molecular orbitals for ferrocene on Cu(100) have smaller binding energies than is the case for ferrocene on Ag(100), the bonding mechanism cannot be elucidated from our photoemission results. It is important to be aware that dehydrogenation can change bonding configurations; for example, *o*-xylene bonding orientation to the surface is dominated by the partial dehydrogenation of the methyl groups.[33]

Substrate-dependent bonding configurations are known for other molecular adsorbates as well. A molecular orientation with the ring parallel with the surface (i.e. a "flat" bonding configuration) has been found for benzene on Pd(100),[34] Pt(111),[35] Rh(111),[36] Ir(111),[37] Ni(111),[38−40] and Ru(100).[41] For benzene on Pd(110)[42,43] the selection rules applied to the angle resolved photoemission measurements suggest that instead of lying "flat" the adsorption geometry is slightly tilted. A tilt geometry of 10°−20° was proposed,[43] reducing the overall symmetry to C_s. Similarly, benzene on Cu(110) is also believed to be tilted[44] to an even greater degree than the 10°−20° inferred for benzene on Pd(110).

The closely related molecule, pyridine, does not lie flat as readily as benzene. Angle-resolved photoemission measurements show quite clearly that the molecule bonds through the N atom on Ir (111).[37] The molecule stands up (i.e., upright), occupying a relatively high point group symmetry in this bonding configuration, with the molecular axis along the surface normal.[37] Angle-resolved photoemission results for pyridine on Pd(111) suggest a tilted configuration (neither "flat" nor "upright" in bonding configuration) with the molecule interacting with the surface through both the nitrogen lone pair electrons and the p electrons.[45] Pyridine on Pd(110) appears from angle-resolved photoemission to bond in a "flat" configuration.[46] This is quite different from many of the results for the pyridine bonding configuration. Angle-resolved photoemission from this surface, Pd(110), has also provided unusual results for benzene, as we have just noted—the bonding of benzene on Pd(110) has been suggested to bond in a tilted configuration (opposite to most benzene bonding configurations).[43]

Conclusion

We find that ferrocene is weakly bound to Ag(100), consistent with earlier studies,[5] and the preferential bonding orientation is with the molecular axis along the surface normal. Molecular ferrocene adsorption on Cu(100), on the other hand, bonds with the molecular axis parallel with the surface and a preferential orientation along the $\langle 1\bar{1}0 \rangle$ direction. Significantly, preliminary results indicate that the differing bonding modes give rise to differing rates of surface decomposition.

The vibrational modes in the HREELS measurements are reasonably well modeled with the extended basis set (3-21G) calculations. The infrared and Raman data available in the literature support our assignments of the vibrational modes from the HREELS data. Nevertheless, the high-frequency peaks require significant improvements in the calculations. We anticipate that the use of anharmonic force field would enhance the accuracy of the results and help us better model the vibrational modes for all the peaks in the HREELS spectrum of ferrocene.

Acknowledgment. This work was supported by the U.S. Department of Energy through Grant DE-FG02-95ER12177.AOOO, the Division of Materials Sciences, U.S. Department of Energy, under Contract DE-AC05-96OR22464 with Lockeed Martin Energy Research Corp., and the donors of Petroleum Research Fund, administered by the American Chemical Society. The authors thank David Pugmire for his careful reading of the manuscript.

References and Notes

(1) Togni, A. *Angew. Chem., Int. Ed. Engl.* **1996**, *35*, 1475. Riant, O.; Samuel, O.; Kagan, H. B.; *J. Am. Chem. Soc.* **1993**, *115*, 5835. Tsukazaki, M.; Tiukl, M.; Rogans, A.; Capell, B. J.; Taylor N. J.; Snieckus, V.; *J. Am. Chem. Soc.* **1996**, *118*, 685. Nishibayashi, Y.; Arikawa, Y.; Ohe K.; Uemura, S.; *J. Org. Chem.* **1996**, *61*, 1172.

(2) Boag, N. M.; Dowben, P. A. Designing Organometallics for Vapor Phase Metallization of Plastics. *Metallized Plastics 4: Fundamental and Applied Aspects*; Mittal, K. L., Ed.; Plenum Press: New York, 1997. Dowben, P. A.; Spencer, J. T.; Stauf, G. T. *Mater. Sci. Eng.* **1989**, *B2*, 297.

(3) Spencer, J. T. *Prog. Inorg. Chem.* **1994**, *41* (Chapter 3), 145−2376. Kodas, T.; Hampden-Smith, M. *The Chemistry of Metal CVD*; VCH Publishers: New York, 1994.

(4) Dormans, G. J. M. *J. Cryst. Growth* **1991**, *108*, 806.

(5) Welipitiya, D.; Dowben, P. A.; Zhang, J.; Pai, W. W.; Wendelken, J. F. *Surf. Sci.* **1996**, *367*, 20.

(6) Welipitiya, D.; Green, A.; Woods, J. P.; Dowben, P. A.; Robertson, B.; Byun, D.; Zhang, J. *J. Appl. Phys.* **1996**, *79*, 8730.

(7) Zanoni, R.; Piancastelli, M. N.; Marsi, M.; Margaritondo, G. *J. Electron Spectrosc. Relat. Phenom.* **1991**, *57*, 199.

(8) Dowben, P. A. *Z. Phys. Chem.*, in press.

(9) Ueno, N. *J. Electron Spectrosc. Relat. Phenom.* **1996**, *78*, 345.

(10) Ueno, N.; Suzuki, K.; Hasegawa, S.; Kamiya, K.; Seki, K.; Inokuchi, H.; *J. Chem. Phys.* **1993**, *99*, 7169. Hasegawa, S.; Tanaka, S.; Tamashita, Y.; Inokuchi, H.; Fujimoto, H.; Kamiaya, K.; Seki, K.; Ueno, N. *Phys. Rev.* **1993**, *B48*, 2596. Yamashita, Y.; Tanaka, S.; Imaeda, K.; Inokuchi, H. *Chem. Phys. Lett.* **1991**, *7*, 1213. Horowitz, G.; Peng, X.; Fichou, D.; Ganier, F. *J. Appl. Phys.* **1990**, *67*, 528. Ishii, H.; Nariaka, S.; Edamatsu, K.; Kamiya, K.; Hasegawa, S.; Ohta, T.; Ueno, N.; Seki, K. *J. Electron Spectrosc. Relat. Phenom.* **1996**, *78*, 395. Yannoulis, P.; Frank, K.-H.; Koch, E. E. *Surf. Sci.* **1991**, *243*, 58. Yannoulis, P.; Frank, K.-H.; Koch, E.-E. *Surf. Sci.* **1991**, *241*, 325.

(11) Lee, S.; Li, D.; Dowben, P. A.; Perkins, F. K.; Onellion, M.; Spencer, J. T. *J. Am. Chem. Soc.* **1991**, *113*, 8444. Zeng, H.; Byun, D.; Zhang, J.; Vidali, G.; Onellion, M.; Dowben, P. A. *Surf. Sci.* **1994**, *313*, 239.

(12) Permien, T.; Engelhardt, R.; Feldmann, C. A.; Koch, E. E. *Chem. Phys. Lett.* **1983**, *98*, 527. Karmiya, K.; Momose, M.; Kitamura, A.; Harada, Y.; Ueno, N.; Miyazaki, T.; Hasegawa, S.; Inokuchi, H.; Narioka, S.; Ishii, H.; Seki, K. *Mol. Cryst. Liq. Cryst.* **1995**, *267*, 211. Richardson, Chem. N. V. *Phys. Lett.* **1983**, *102*, 390.

(13) Dowben, P. A.; LaGraffe, D.; Onellion, M. *J. Phys.: Condens. Matter* **1989**, *1*, 6571.

(14) Gaussian 92, Revision G.3: Frisch, M. J.; Trucks, G. W.; Schlegel, H. B.; Gill, P. M. W.; Johnson, B. G.; Wong, M. W.; Foresman, J. B.;

Robb, M. A.; Head-Gordon, M.; Replogle, E. S.; Gomperts, R.; Andres, J. L.; Raghavachari, K.; Binkley, J. S.; Gonzalez, C.; Martin, R. L.; Fox, D. J.; Defrees, D. J.; Baker, J.; Stewart, J. J. P.; Pople, J. A. Gaussian Inc., Pittsburgh, PA, 1993.

(15) Hehre, W. J.; Radom, L.; Schleyer, P. V. R.; Pople, J. A. *Ab Initio Molecular Orbital Theory*, Wiley-Interscience: New York, 1985.

(16) Bagus, P. S.; Waldren, U. I.; Almlof, J. *J. Chem. Phys.* **1976**, *64*, 2324.

(17) Coutiere, M.-M.; Demuynck, J.; Veillard, A. *Theor. Chim. Acta* **1972**, *27*, 281.

(18) Rösch, N.; Johnson, K. H. *Chem. Phys. Lett.* **1974**, *24*, 179.

(19) Rösch, N.; Jörg, H. *J. Chem. Phys.* **1986**, *84*, 5967.

(20) Baerends, E. J.; Ros., P. *Chem. Phys. Lett.* **1973**, *23*, 341.

(21) Kirchner, R. F.; Loew, G. H.; Mueller-Westerhoff, U. T. *Theor. Chim. Acta* **1976**, *41*, 1.

(22) Armstrong, D. R.; Fortune, R.; Perkins, P. G. *J. Organomet. Met. Chem.* **1976**, *111*, 197.

(23) Evans, S.; Green, M. L. H.; Jewitt, B.; King, G. H.; Orchard, A. F. *J. Chem. Soc., Faraday Trans. 2* **1973**, 356. Evans, S.; Green, M. L. H.; Jewitt, B.; Orchard, A. F.; Pygall, C. F. *J. Chem. Soc., Faraday Trans. 2* **1972**, *68*, 1847.

(24) Vondrak, T. *J. Organomet. Chem.* **1984**, *275*, 93.

(25) Rabalais, J. W.; Werme, L. O.; Bergmark, T.; Karson, L.; Hussain, M.; Siegbahn, K. *J. Chem. Phys.* **1972**, *57*, 1185.

(26) Driscoll, D. C.; Dowben, P. A.; Boag, N. M.; Grade, M.; Barfuss, S. *J. Chem. Phys.* **1986**, *85*, 4802. Barfuss, S.; Grade, M.; Hirschwald, W.; Rosinger, W.; Boag, N. M.; Driscoll, D. C.; Dowben, P. A. *J. Vac. Sci. Technol.* **1987**, *A5*, 1451.

(27) Cauletti, C.; Green, J. C.; Kelly, M. R.; Powell, P.; van Tilborg, J.; Robbins, J.; Smart, J. *J. Electron Spectrosc. Relat. Phenom.* **1980**, *19*, 327.

(28) Lippincott, E. R.; Nelson, R. D. *Spectrochim. Acta* **1958**, *10*, 307R.

(29) Schettino, V.; Marzocchi, M. P.; Califano, S. *J. Chem. Phys.* **1969**, *51*, 52645.

(30) Hyams, I. J. *Spectrochim. Acta* **1973**, *29A*, 839.

(31) Aleksanyan, V. T.; Greenwald, I. I. *J. Mol. Struct. (THEOCHEM)* **1982**, 90, 35. Aleksanyan, V. T.; Arsen′eva, T. I.; Vishinsky, N. N.; Greenwald, I. I.; Smirnov, A. S. *Isv. Akad. Nauk SSR Ser. Kim.* **1981**, 297.

(32) Pugmire, D.; Woodbridge, C.; Langell, M. Manuscript in preparation.

(33) Wilk, D. E.; Stanners, C. D.; Shen, Y. R.; Somorjai, G. A. *Surf. Sci.* **1993**, *280*, 298.

(34) Hoffman, P.; Horn, K.; Bradshaw, A. M. *Surf. Sci.* **1981**, *105*, L260. Nyberg, G. L.; Richardson, N. V. *Surf. Sci.* **1979**, *85*, 335.

(35) Freund, H. J.; Eberhardt, W.; Heskett, D.; Plummer, E. W. *Phys. Rev. Lett.* **1983**, *50*, 768.

(36) Neumann, M.; Mack, J. U.; Bertel, E.; Netzer, F. P. *Surf. Sci.* **1985**, *155*, 629. Bertel, E.; Rosina, G.; Netzer, F. P. *Surf. Sci.* **1986**, *172*, L515.

(37) Mack, J. U.; Bertel, E.; Netzer, F. P. *Surf. Sci.* **1985**, *159*, 265.

(38) Huber, W.; Steinrück, H.-P.; Pache, T.; Menzel, D. *Surf. Sci.* **1991**, *217*, 103.

(39) Huber, W.; Zebisch, P.; Bornemann, T.; Steinrück, H.-P. *Surf. Sci.* **1991**, *258*, 16.

(40) Steinrück, H.-P. *Appl. Phys.* **1994**, *A59*, 517.

(41) Heimann, P. A.; Jacob, P.; Pache, T.; Steinrück, H.-P.; Menzel, D. *Surf. Sci.* **1989**, *210*, 282.

(42) Netzer, F. P.; *Vacuum* **1990**, *41*, 49.

(43) Netzer, F. P.; Rangelov, G.; Rosina, G.; Saalfeld, H. B.; Neumann, M.; Lloyd, D. R. *Phys. Rev.* **1988**, *B37*, 10399.

(44) Lomas, J. R.; Baddeley, C. J.; Tikhov, M. S.; Lambert, R. M. *Chem. Phys. Lett.* **1996**, *263*, 591.

(45) Netzer, F. P.; Mack, J.-U. *Chem. Phys. Lett.* **1983**, *95*, 492.

(46) Netzer, F. P.; Rangelov, G.; Rosina, G.; Saalfeld, H. B. *J. Chem. Phys.* **1988**, *89*, 3331.

(47) Brunvoll, J.; Cyvin, C. J.; and Schäfer, L. *J. Organomet. Chem.* **1971**, *27*, 107.